1-1-2012

Electrochemical characteristics of layered Li1.95Mn0.9Co0.15O3 (C2/m) as a lithium-battery cathode

Kiyoshi Ozawa
National Institute for Materials Science, ozawa@uow.edu.au

Yasuhiro Nakao
Honda Engineering Co., Ltd

Takashi Mochiku
National Institute for Materials Science

Zhenxiang Cheng
University of Wollongong, cheng@uow.edu.au

Lianzhou Wang
University of Queensland

See next page for additional authors

Electrochemical Characteristics of Layered $Li_{1.95}Mn_{0.9}Co_{0.15}O_3$ (*C*2/*m*) as a Lithium-Battery Cathode

Kiyoshi Ozawa, Yasuhiro Nakao, Takashi Mochiku, Zhenxiang Cheng, Lianzhou Wang, Hideo Iwai, Yoshinori Tsuchiya, Hiroki Fujii and Naoki Igawa

J. Electrochem. Soc. 2012, Volume 159, Issue 3, Pages A300-A304.
doi: 10.1149/2.079203jes

Journal of The Electrochemical Society, **159** (3) A300-A304 (2012)
0013-4651/2012/159(3)/A300/5/$28.00 © The Electrochemical Society

Electrochemical Characteristics of Layered $Li_{1.95}Mn_{0.9}Co_{0.15}O_3$ (*C*2/*m*) as a Lithium-Battery Cathode

Kiyoshi Ozawa,[a,z] Yasuhiro Nakao,[b] Takashi Mochiku,[a] Zhenxiang Cheng,[c] Lianzhou Wang,[d] Hideo Iwai,[a] Yoshinori Tsuchiya,[a] Hiroki Fujii,[a] and Naoki Igawa[e]

[a]*National Institute for Materials Science, Tsukuba, Ibaraki 305-0047, Japan*
[b]*Honda Engineering Co., Ltd., Haga-Machi, Haga-Gun, Tochigi 321-3395, Japan*
[c]*Institute for Superconducting & Electronic Materials, University of Wollongong, NSW 2522, Australia*
[d]*ARC Centre for Excellence for Functional Nanomaterials, School of Chemical Engineering and AIBN, The University of Queensland, St Lucia QLD 4072, Australia*
[e]*Quantum Beam Science Directorate, Japan Atomic Energy Agency, Tokai-mura, Ibaraki 319-1195, Japan*

A manganese-based solid solution with the composition of $Li_{1.95}Mn_{0.9}Co_{0.15}O_3$ was synthesized by a simplified coprecipitation method, followed by a combustion technique, and its electrochemical characteristics as a lithium-battery cathode were investigated. Rietveld refinement based on neutron diffraction data revealed that the material is assigned to an Li_2MnO_3-type structure model with a monoclinic cell due to the space group symmetry of *C*2/*m*. In cycling of the $Li/Li^+/Li_{1.95}Mn_{0.9}Co_{0.15}O_3$ cell in the potential range of 2.0–4.8 V at current densities of 30 mAg^{-1}, the discharge capacity characteristically increases from 46.3 to 196.5 $mAhg^{-1}$ as the cycle increases from 1 to 11, and a discharge capacity of >175.5 $mAhg^{-1}$ is obtained between the 23rd and 58th cycles with small capacity fading of 2.41%. The results of cyclic voltammogram (CV) and X-ray photoelectron spectroscopy (XPS) measurements showed that the manganese redox reaction (Mn^{3+}/Mn^{4+}) in the $Li_{1.95}Mn_{0.9}Co_{0.15}O_3$ system is progressively activated during the first ten-odd cycles, following continuous occurrence of the extraction of oxygen molecules from the electrode material over these charge processes. It could be assumed that such behaviors significantly influence the electrochemical characteristics of the $Li_{1.95}Mn_{0.9}Co_{0.15}O_3$ system.
 [DOI: 10.1149/2.079203jes]

Manuscript submitted October 20, 2011; revised manuscript received November 16, 2011. Published January 10, 2012.

In the past two decades, considerable efforts have been devoted to the development of rechargeable energy-storage devices that can be used in diversified technical applications, expanding over to portable electronics, electric cars, and large-scale industrial equipments. Lithium-ion batteries, which can realize a high energy density, are a promising candidate for such devices. The performance of lithium-ion batteries shows considerable fluctuation depending on that of the cathode materials, as a result of which much attention has focused on the various kinds of lithiated transition-metal oxides for their possible use as a promising cathode material. Layered compounds, such as $LiCoO_2$ and $LiNiO_2$, have been significantly studied as a high-voltage cathode material. However, their high cost and safety hazard have inhibited their use in a wide range of applications. In contrast, olivine-type $LiFePO_4$ does not carry these problems, but the available capacities are reaching its theoretical limit.

Manganese-based layered oxides, such as $LiMnO_2$ (*C*2/*m* or *Pmnm*),[1–3] Li_2MnO_3 (*C*2/*m*),[4] and solid solutions of Li_2MnO_3-$LiMO_2$ (M = Ni, Co, and Mn: $R\bar{3}m$),[5–9] are attractive materials because they are safer, cheaper, and less toxic than $LiCoO_2$ or $LiNiO_2$ and exhibit a higher operating voltage (>3.5 V vs. Li/Li^+ in average). Especially, much attention has been increasingly placed on the solid solutions of Li_2MnO_3-$LiMO_2$ due to their high capacities. Recently, Yabuuchi et al.[8] reported that the high capacities of the Li_2MnO_3-$LiMO_2$ systems result from the activated manganese redox reaction (Mn^{3+}/Mn^{4+}) and the oxygen reduction reaction at the electrode surface. However, the need for improvement in their capacity retention is also recognized when they are used in practical applications.

The charge-discharge behaviors of Li_2MnO_3-$LiMO_2$ systems are characterized by an irreversible high charge capacity (>300 $mAhg^{-1}$) for the first charge process. This is because of the extraction of oxygen molecules from the electrode materials. While such an extraction leads to the activated manganese redox reaction, it is a major cause of a poor cycle life of the systems. The rapid generation of oxygen vacancies causes the structural destruction of active materials, and a poor cycle life is thus induced. To suppress structural destruction, several surface modifications of the electrode materials, such as acid treatment with an aqueous H_2SO_4 solution[10] and surface coating with $AlPO_4$[11] or TiO_2,[12] have been reported.

Recently, we have synthesized a manganese-based solid solution having the composition of $Li_{1.95}Mn_{0.9}Co_{0.15}O_3$ due to the space group symmetry of *C*2/*m*. It was found that the material shows unique and favorable electrochemical characteristics as a lithium-battery cathode, i.e., an increasing capacity during the first ten-odd cycles and improved capacity retention after around the 23rd cycle in the charge-discharge potential range of 2.0–4.8 V. In this paper, we describe the synthesis and structure of the material and then discuss its electrochemical properties.

Experimental

Synthesis of the material.— $Li_{1.95}Mn_{0.9}Co_{0.15}O_3$ was synthesized from a mixed manganese-cobalt carbonate precursor which was obtained by the coprecipitation technique based on a modification of previously reported methods.[6,7] Manganese sulfate ($MnSO_4 \cdot 5H_2O$) and cobalt sulfate ($CoSO_4 \cdot 7H_2O$) were weighed to achieve a molar ratio of Co/Mn = 0.15/0.9 and dissolved in distilled water to obtain a 0.2 M aqueous solution of manganese and cobalt sulfates. The solution was added to an aqueous solution of sodium carbonate (Na_2CO_3) containing an equimolar amount of Na_2CO_3 with manganese and cobalt sulfates and stirred for about 20 h. The produced green precipitate in the solution was then filtered with suction through a 0.2-μm pore size polytetrafluoroethylene (PTFE) membrane, thoroughly washed with distilled water, and dried at 110°C to yield the manganese-cobalt carbonate coprecipate. The resulting coprecipitate was heated at 500°C in air for 5 h, thoroughly mixed with lithium hydroxide ($LiOH \cdot H_2O$), and finally heated at 900°C for 12 h under flowing oxygen to obtain the $Li_{1.95}Mn_{0.9}Co_{0.15}O_3$ material.

Characterization.— Neutron-diffraction data were collected by monochronized neutron radiation at a wavelength of 1.8244 Å at room temperature using a high-resolution powder diffractometer (HRPD) at the research reactor (JRR-3M) of the Japan Atomic Energy Agency. The synthesized powder (about 5 g) was contained in a cylindrical vanadium cell (5-mm radius, 55-mm height). Based on the neutron-diffraction data, the structural parameters of $Li_{1.95}Mn_{0.9}Co_{0.15}O_3$ were refined using the Rietveld refinement program RIETAN-FP.[13]

[z] E-mail: OZAWA.Kiyoshi@nims.go.jp

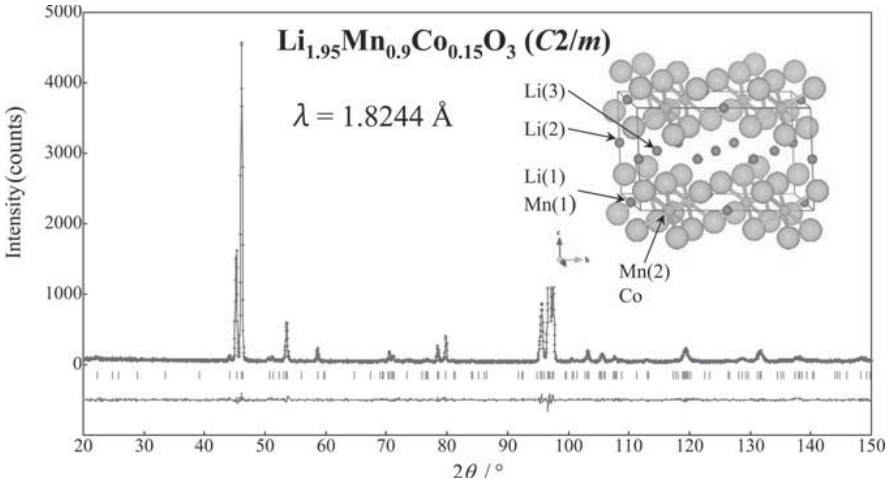

Figure 1. Rietveld refinement pattern of the neutron-diffraction data measured for $Li_{1.95}Mn_{0.9}Co_{0.15}O_3$. The plus marks (+) are the raw diffraction data, and the overlapped continuous line is the calculated pattern. The short vertical lines below the pattern indicate the positions of the allowed Bragg reflections. The difference between the observed and calculated intensities is shown at the bottom on the same scale. An *ac* plane projection of the structure is also shown.

Powder X-ray diffraction (XRD) measurements were also performed for the as-prepared material and cycled cathode samples using an X-ray diffractometer (Rigaku RINT-TTR III). In addition, an X-ray photoelectron spectroscopy (XPS) measurement was also carried out on the as-prepared material and cathode samples after charge-discharge cycles using the PHI Quantera SXM spectrometer (ULVAC-PHI).

Electrochemical test.— Electrochemical charge-discharge measurements were carried out using a 2032-type coin cell. The electrolyte was a 1 M solution of $LiPF_6$ in ethylene carbonate (EC) and diethyl carbonate (DEC) mixed at a volume ratio of 1: 1 (Ube Industries, Ltd., Japan). The anode was a lithium metal foil disk (11-mm diameter, 0.5-mm thickness). A polypropylene filter was used as the separator. The cathodes were comprised of an aluminum grid on which the finely ground powder of the samples, mixed with 15 wt% carbon black and 10 wt% PTFE powders, was pressed; these cathodes were dried at 140°C for 4 h under a vacuum immediately before the measurements. The charge-discharge measurements were carried out in the potential ranges of 2.0–4.8 and 2.0–4.6 V at current densities of $\pm 30\ mAg^{-1}$ or $\pm 10\ mAg^{-1}$ and 23°C. Every charge-discharge cycling in this study began from the charge process. Cyclic voltammogram (CV) measurements were also conducted in the potential ranges of 2.0–4.8 and 2.0–4.6 V at the scan rate of $0.2\ mVs^{-1}$ using potentiostat equipment (Bio-Logic VSP Modular).

Table I. Rietveld refinement results for $Li_{1.95}Mn_{0.9}Co_{0.15}O_3$ with neutron diffraction data measured at room temperature.

		Atomic positions				
Atom	Site	*x*	*y*	*z*	g^a	B^b(Å^2)
Li1	2*b*	0	1/2	0	0.9	1.0(3)
Mn1	2*b*	0	1/2	0	0.1	$= B_{Li1}$
Li2	2*c*	0	0	1/2	1.0	0.7(3)
Li3	4*h*	0	0.662(2)	1/2	1.0	1.6(2)
Mn2	4*g*	0	0.1674(10)	0	0.85	0.1(1)
Co	4*g*	0	$= y_{Mn2}$	0	0.15	$= B_{Mn2}$
O1	4*i*	0.2249(8)	0	0.2262(9)	1.0	0.74(8)
O2	8*j*	0.2500(6)	0.3250(3)	0.2219(5)	1.0	0.83(4)

Lattice parameters: $a = 4.9289(3)$ Å, $b = 8.5321(3)$ Å, $c = 5.0248(2)$ Å, $\beta = 109.270(3)°$
Reliability factors: $R_{wp} = 9.92\%$, $R_p = 7.08\%$, $R_R = 15.05\%$, $R_B = 3.24\%$, $R_F = 4.38\%$, $R_e = 10.45\%$
[a] Occupancy factor
[b] Isotropic atomic displacement parameter

Results and Discussion

The results of the Rietveld refinement for $Li_{1.95}Mn_{0.9}Co_{0.15}O_3$ with the neutron-diffraction data are summarized in Fig. 1 and Table I. The best fit was realized by setting the atomic distributions to those due to an Li_2MnO_3-type structure model corresponding to a monoclinic symmetry with the space group of *C*2/*m* ($z = 4$).[14] All the Bragg reflections can be indexed on such a monoclinic cell, and both low *R* factors (Table I) and good fitting between the observed and calculated patterns (Fig. 1) are acquired. It is noted that the substitution of Mn for Li characteristically occurs on the *ab* plane with $z = 0$ in the $Li_{1.95}Mn_{0.9}Co_{0.15}O_3$. It should be also pointed out that refinements employing structure models other than the Li_2MnO_3-type structure, such as a model based on the $R\bar{3}m$ symmetry, did not converge or led to poorer convergence. The results of the Rietveld refinement ensure the validity of the Li_2MnO_3-type structure model.

Figure 2 shows the charge and discharge curves at the 1st, 2nd, 3rd, 22nd, and 58th cycles measured with the $Li/Li^+/Li_{1.95}Mn_{0.9}Co_{0.15}O_3$ cell in the potential range of 2.0–4.8 V at current densities of $\pm 30\ mAg^{-1}$. Small irreversibility is observed at the 1st, 2nd, and 3rd cycles, in which the charge capacity is slightly larger than the discharge one. At the 22nd and 58th cycles, symmetrical charge and discharge curves with an enhanced capacity of $\sim 180\ mAhg^{-1}$ are observed, suggesting the occurrence of a reversible electrochemical reaction at those cycles. It is important to note that these charge and discharge curves are markedly different from those reported for conventional Li_2MnO_3-$LiMO_2$ (M = Ni, Co, and Mn) systems, in which

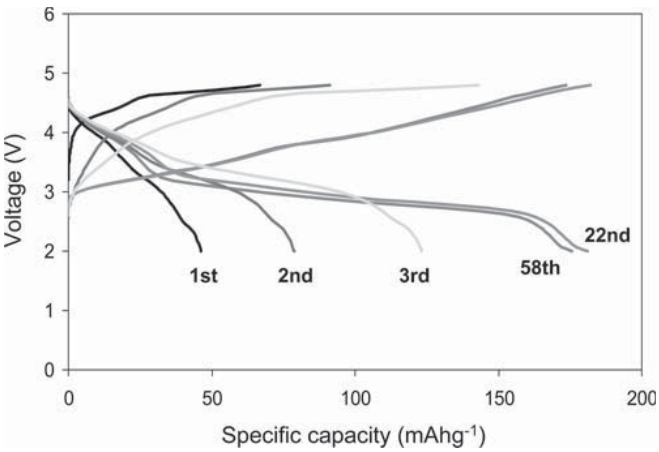

Figure 2. Charge and discharge curves of the 1st, 2nd, 3rd, 22nd, and 50th cycles measured with the $Li/Li^+/Li_{1.95}Mn_{0.9}Co_{0.15}O_3$ cell in the potential range of 2.0–4.8 V at current densities of $\pm 30\ mAg^{-1}$.

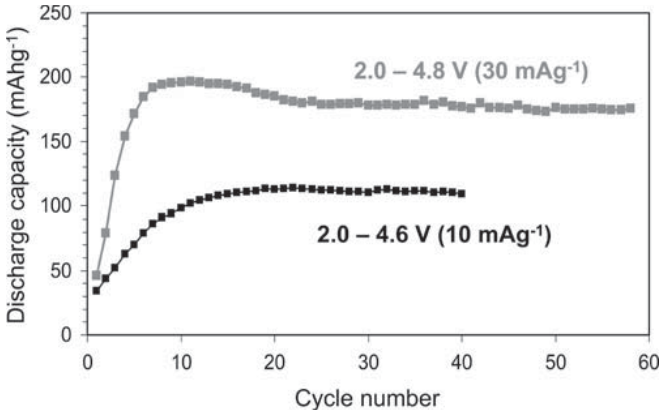

Figure 3. Cycling data measured with the $Li/Li^+/Li_{1.95}Mn_{0.9}Co_{0.15}O_3$ cell in the potential ranges of 2.0–4.8 and 2.0–4.8 V at current densities of ±30 or ±10 mAg^{-1}.

an irreversible long plateau with a high capacity (>250 $mAhg^{-1}$) develops at 4.5–4.6 V for the first charge process.[7] As discussed below, the difference in the charge-discharge behaviors between the systems is associated with their activation behaviors of the manganese redox reaction (Mn^{3+}/Mn^{4+}) during the cycling.

Figure 3 shows the cycling data measured with the $Li/Li^+/Li_{1.95}Mn_{0.9}Co_{0.15}O_3$ cell in the potential ranges of 2.0–4.8 and 2.0–4.6 V, in which the discharge capacities are plotted as a function of the number of cycles. For the potential range of 2.0–4.8 V, the capacity characteristically increases from 46.3 to 196.5 $mAhg^{-1}$ as the cycle increases from 1 to 11 and then slightly decreases to 179.8 $mAhg^{-1}$ until the 23rd cycle. Subsequently, capacities of >175.5 $mAhg^{-1}$ are obtained up to the 58th cycle with only a slight decrease. In fact, capacity fading between the 23rd and 58th cycles is 2.41%. Here, it may be noted that the capacities of >175.5 $mAhg^{-1}$ and capacity retention observed between the 23rd and 58th cycles seem to be superior to those reported for the conventional solid solution of $0.6Li_2MnO_3$-$0.1LiCoO_2$ ($R\bar{3}m$), which has the same composition of $Li_{1.95}Mn_{0.9}Co_{0.15}O_3$.[5,9] For the potential range of 2.0–4.6 V, although the capacity increased to ∼110 $mAhg^{-1}$ during the first ten-odd cycles, the subsequent capacities do not exceed 113 $mAhg^{-1}$.

In order to investigate the redox reactions of the $Li_{1.95}Mn_{0.9}Co_{0.15}O_3$ system during the cycling, we conducted CV measurements in two types of potential ranges: 2.0–4.8 and 2.0–4.6 V. Figure 4 shows the resulting CVs measured with the $Li/Li^+/Li_{1.95}Mn_{0.9}Co_{0.15}O_3$ cell at the scan rate of 0.2 mVs^{-1} over 15 or 16 cycles. Compared with the CVs shown in Fig. 4a and 4b, there are significant differences in the CV variation for the respective potential ranges. For the potential range of 2.0–4.8 V (Fig. 4a), the CV loop becomes increasingly larger as the number of cycles increases. Especially, a remarkable enlargement in size is observed for the peak at around 3.0 V in the reduction process during the first ten-odd cycles. In contrast, the peak at around 4.0 V in the reduction process rarely changes in size during the cycling. The former and latter peaks can be assumed to result from the manganese redox reaction (Mn^{3+}/Mn^{4+}) and the cobalt redox reaction (Co^{3+}/Co^{4+}), respectively.[15] For the potential range of 2.0–4.6 V (Fig. 4b), an enlarging trend of the CV loop is also observed, but the variation is considerably smaller than that seen in Fig. 4a. These observations show that the manganese redox reaction of the $Li_{1.95}Mn_{0.9}Co_{0.15}O_3$ system is progressively activated upon cycling and the stage of activation is also associated with the maximum voltage for the charge process, in a similar manner to the variation of the capacities.

We carried out another CV measurement to further investigate the relationship between the manganese redox reaction and the charge-discharge conditions. Figure 5 shows CVs measured with the $Li/Li^+/Li_{1.95}Mn_{0.9}Co_{0.15}O_3$ cell in the potential range of

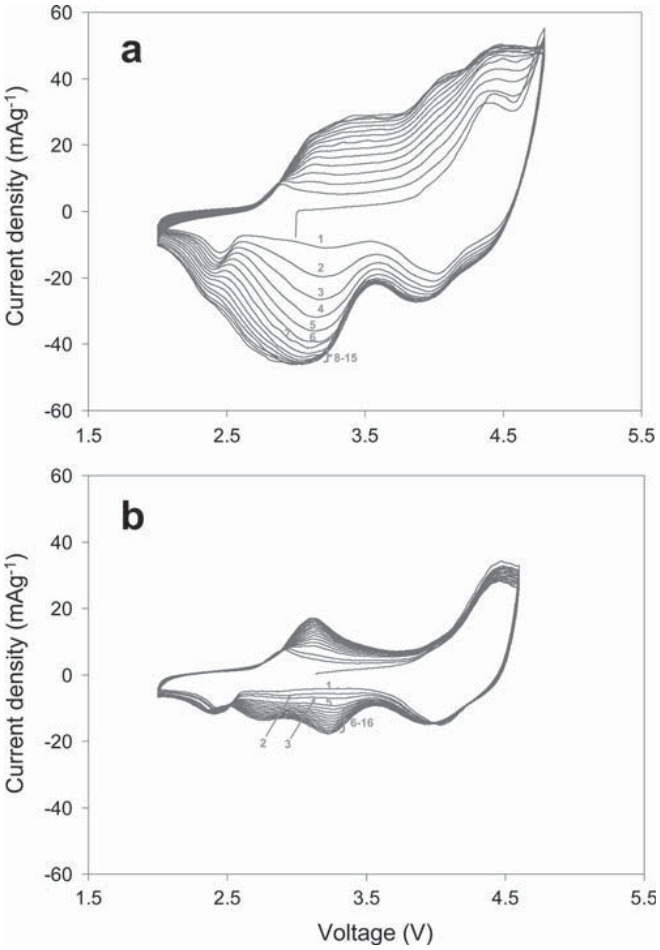

Figure 4. Cyclic voltammograms measured with the $Li/Li^+/Li_{1.95}Mn_{0.9}Co_{0.15}O_3$ cell in the potential ranges of 2.0–4.8 (a) and 2.0–4.6 V (b) over 15 or 16 cycles at the scan rate of 0.2 mVs^{-1}.

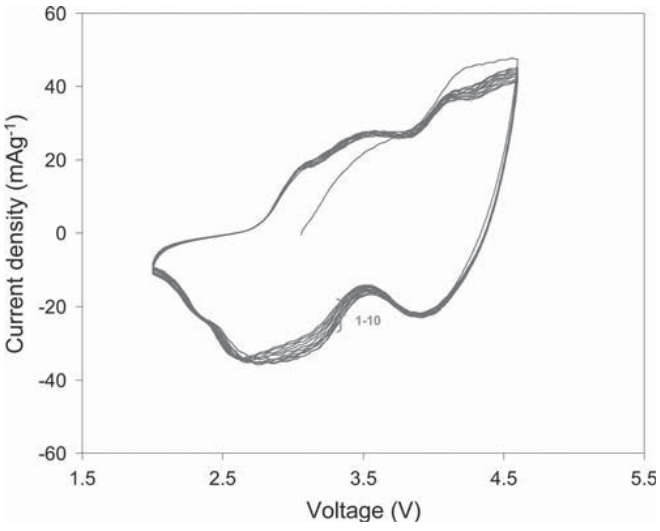

Figure 5. Cyclic voltammograms measured with the $Li/Li^+/Li_{1.95}Mn_{0.9}Co_{0.15}O_3$ cell in the potential ranges of 2.0–4.6 V over 10 cycles at the scan rate of 0.2 mVs^{-1}. The cell was previously charge-discharged in the potential range of 2.0–4.8 V at current densities of 30 mAg^{-1} over 15 cycles before the measurement.

2.0–4.6 V at the scan rate of 0.2 mVs^{-1} over 10 cycles; it must be noted that the cell was previously charge-discharged in the potential range of 2.0–4.8 V over 15 cycles before the measurement. An enlarged CV loop with almost no change in size, which closely resembles that observed after ten-odd cycles in Fig. 4a, is detected over the entire cycles. These events suggest that the activated manganese redox reaction once induced in the $Li_{1.95}Mn_{0.9}Co_{0.15}O_3$ system could be maintained even if the potential range was changed.

XPS measurements were carried out for the as-prepared $Li_{1.95}Mn_{0.9}Co_{0.15}O_3$ and the electrode samples after 5 and 10 cycles in the potential range of 2.0–4.8 V; it is noted that all the samples were washed with acetone and then dried at 120°C for 1 h under a vacuum immediately before the measurements. The XPS core spectra with respect to the O, Co, and Mn components are shown in Fig. 6. The spectrum position of O 1s shifts to a lower binding energy as the number of cycles increases; while the top position of the as-prepared material is 529.0 eV, the positions of 5- and 10-cycled samples are 530.5 and 531.5 eV, respectively (Fig. 6a). It has been reported that the binding energy of O 1s varies according to the chemical species and the values for oxygen ion (O^{2-}) in the crystal lattice and free oxygen ions based on Li_2O or Li_2CO_3 are 529 and 532 eV, respectively.[8,16,17] Thus, it was suggested that oxygen molecules in the $Li_{1.95}Mn_{0.9}Co_{0.15}O_3$ system are extracted from the active material during the cycling and the extracted oxygen exists at the electrode surface. In addition, since the position of the 10-cycled sample is higher than those of the as-prepared material and 5-cycled sample, it was also suggested that continual extraction of oxygen molecules occurs, at least during the first ten cycles. The binding energies of Co $2p_{1/2}$ and Co $2p_{3/2}$ for the as-prepared material are estimated to be 795.2 and 779.5 eV, respectively (Fig. 6b). These values coincide with those reported in $LiCoO_2$,[17] suggesting the 3+ charge state of Co in the as-prepared material. The binding energies of Mn $2p_{1/2}$ and Mn $2p_{3/2}$ in the as-prepared material are estimated to be 653.9 and 642.2 eV, respectively (Fig. 6c). These values are almost consistent with those reported in MnO_2,[18] which indicates that the charge state of Mn is

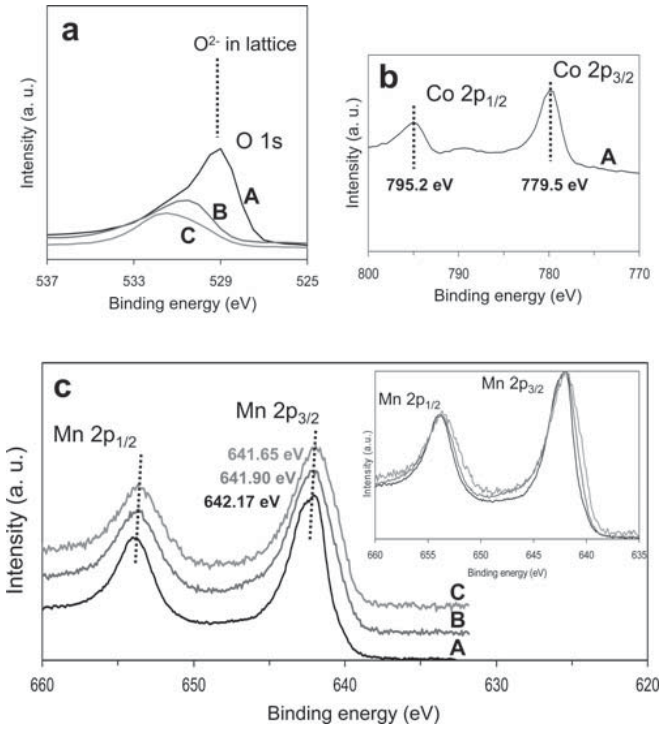

Figure 6. XPS core spectra of O (a), Co (b), and Mn (c) for the as-prepared $Li_{1.95}Mn_{0.9}Co_{0.15}O_3$ (A), 5-cycled cathode sample (B), and 10-cycled cathode sample (C). The charge-discharge cycles were carried out in the potential range of 2.0–4.8 V at current densities of ± 30 mAg^{-1}.

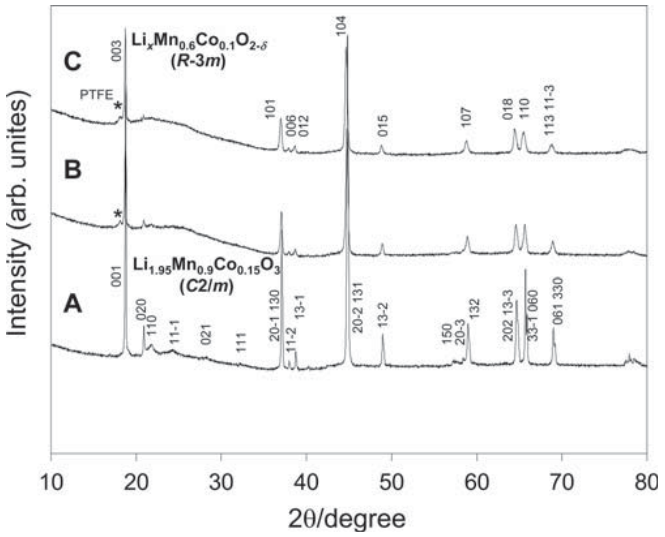

Figure 7. XRD profiles of the as-prepared $Li_{1.95}Mn_{0.9}Co_{0.15}O_3$ (A), 5-cycled cathode sample (B), and 10-cycled cathode sample (C). The charge-discharge cycles were carried out in the potential range of 2.0–4.8 V at current densities of ± 30 mAg^{-1}.

4+ in the as-prepared material. It can also be observed in Fig. 6c that the spectrum positions of both Mn $2p_{1/2}$ and Mn $2p_{3/2}$ slightly shift to lower binging energies as the number of cycles increase. Additionally, as shown in the inset of the figure, the spectra become more asymmetrical due to swelling toward lower binding energies. These observations indicate that the quantity of Mn^{3+} in the active material increases as the number of cycles increases,[18] which is in agreement with the CV results.

Figure 7 shows the XRD profiles of the as-prepared material and 5- and 10-cycled cathode samples in the potential range of 2.0–4.8 V at current densities of ± 30 mAg^{-1}. For the as-prepared material, all the Bragg reflections can be assigned to those reported for the Li_2MnO_3 (*C*2/*m*).[19] On the other hand, for the cycled samples, profiles are substantially changed to that for the $LiMnO_2$ ($R\bar{3}m$).[20] Especially, the profile of the 10-cycled sample is shown to be almost a single phase of the $LiMnO_2$. It could be assumed that the structural change from *C*2/*m* to $R\bar{3}m$ during the cycling is responsible for the reduction of crystal distortion due to the irreversible extraction of Li^+ ions at the 2*b* site.

For manganese-based cathode materials, it is commonly accepted that electrochemical Li^+ extraction occurs in conjunction with the oxidation of Mn up to a maximum oxidation state of 4+. Since the charge state of Mn is already 4+ in $Li_{1.95}Mn_{0.9}Co_{0.15}O_3$, the small charge and discharge capacities observed at the first cycle in the $Li_{1.95}Mn_{0.9}Co_{0.15}O_3$ system can be understood in terms of this concept. In other words, the capacities at the first cycle are mostly caused by the Li^+ extraction and insertion accompanying the redox reaction of cobalt (Co^{3+}/Co^{4+}). On the other hand, the CV and XPS results suggest that the high capacities obtained after ten-odd cycles in the $Li_{1.95}Mn_{0.9}Co_{0.15}O_3$ system refer to the enhanced Li^+ extraction and insertion based on the activated manganese redox reaction (Mn^{3+}/Mn^{4+}) following the extraction of oxygen molecules from the active material, as reported for Li_2MnO_3-$LiMO_2$ systems. Furthermore, taking into account the structural variation shown in Fig. 7, the difference in the capacity retention between the $Li_{1.95}Mn_{0.9}Co_{0.15}O_3$ and Li_2MnO_3-$LiMO_2$ systems would be related to their extraction behaviors of oxygen molecules. The oxygen extraction is generally completed for the first charge process in Li_2MnO_3-$LiMO_2$ systems, whereas it continuously occurs over the first ten-odd charge processes in the $Li_{1.95}Mn_{0.9}Co_{0.15}O_3$ system. Such an extraction behavior in the $Li_{1.95}Mn_{0.9}Co_{0.15}O_3$ system may probably suppress the structural destruction due to the generation of oxygen vacancies and thus

contribute to the improved capacity retention. However, a full discussion of these aspects must await a detailed comparison of the microstructures at various electrochemical stages for both systems.

Conclusions

In this paper, we have described the synthesis of a manganese-based solid solution of $Li_{1.95}Mn_{0.9}Co_{0.15}O_3$ and discussed its structural and electrochemical characteristics. The material is assigned to an Li_2MnO_3-type structure model characterized by a monoclinic cell due to the space group symmetry of $C2/m$. Unlike the conventional solid solutions of Li_2MnO_3-$LiMO_2$ (M = Ni, Co, and Mn: $R\bar{3}m$), the material shows more favorable electrochemical properties as a lithium-battery cathode, namely, higher capacities and improved capacity retention after around the 23rd cycle. Such electrochemical properties may probably be associated with the extraction behavior of oxygen molecules from the active material during the cycling in the $Li_{1.95}Mn_{0.9}Co_{0.15}O_3$ system. The electrochemical characteristics observed in the $Li_{1.95}Mn_{0.9}Co_{0.15}O_3$ system may be useful for designing manganese-based cathode materials for practical applications.

Acknowledgments

This work was financially supported by a grant-in-Aid for Scientific Research from the Ministry of Education, Culture, Sport, Science, and Technology in Japan and performed under the Shared Facility Use Program of JAEA (Japan Atomic Energy Agency).

References

1. X. Y. Tu and K. Y. Shu, *J. Solid State Electrochem.*, **12**, 245 (2008).
2. J. Molenda, M. Ziemnicki, J. Marzec, W. Zając, M. Molenda, and M. Bućko, *J. Power Sources*, **173**, 707 (2007).
3. A. R. Armstrong, A. D. Robertson, R. Gitzendanner, and P. G. Bruce, *J. Solid State Chem.*, **145**, 549 (1999).
4. A. D. Robertson and P. G. Bruce, *Chem. Mater.*, **15**, 1984 (2003).
5. J.-M. Kim, S. Tsuruta, and N. Kumagai, *Electrochem. Commun.*, **9**, 103 (2007).
6. K. Numata, C. Sakai, and S. Yamanaka, *Sold State Ionics*, **117**, 257 (1999).
7. A. R. Armstrong, M. Holzapfel, P. Novák, C. S. Johnson, S.-H. Kang, M. M. Thackeray, and P. G. Bruce, *J. Am. Chem. Soc.*, **128**, 8694 (2006).
8. N. Yabuuchi, K. Yoshii, S.-T. Myung, I. Nakai, and S. Komaba, *J. Am. Chem. Soc.*, **133**, 4404 (2011).
9. Y. J. Park, Y.-S. Hong, X. Wu, M. G. Kim, K. S. Ryu, and S. H. Chang, *J. Electrochem. Soc.*, **151**, A720 (2004).
10. C. S. Johnson, J.-S. Kim, C. Lefief, N. Li, J. T. Vaughey, and M. M. Thackeray, *Electrochem. Commun.*, **6**, 1085 (2004).
11. Y. Wu, A. V. Murugan, and A. Manthiram, *J. Electrochem. Soc.*, **155**, A635 (2008).
12. J. M. Zheng, J. Li, Z. R. Zhang, X. J. Guo, and Y. Yang, *Solid State Ionics*, **179**, 1794 (2008).
13. F. Izumi and K. Momma, *Solid State Phenomena*, **130**, 15 (2007).
14. P. Strobel and B. Lambert-Andron, *J. Solid State Chem.*, **75**, 90 (1988).
15. C. Gan, X. X. Hu, H. Zhan, and Y. Zhou, *Solid State Ionics*, **176**, 687 (2005).
16. Y. P. Yu, X. J. Xing, L. M. Xu, S. X. Wu, and S. W. Li, *J. Appl. Phys.*, **105**, 123535 (2009).
17. S. Madhavi, G. V. Subba Rao, B. V. R. Chowdari, and S. F. Y. Li, *J. Electrochem. Soc.*, **148**, A1279 (2001).
18. G. C. Allen, S. J. Harris, and J. A. Jutson, *Appl. Sur. Sci.*, **37**, 111 (1989).
19. Y. S. Meng, G. Ceder, C. P. Grey, W.-S. Yoon, M. Jiang, J. Bréger, and Y. Shao-Horn, *Chem. Mater.*, **17**, 2386 (2005).
20. A. R. Armstrong, N. Dupre, A. J. Paterson, C. P. Grey, and P. G. Bruce, *Chem. Mater.*, **16**, 3106 (2004).